Control over the Hydrophilicity in the Pores of Covalent Organic Framework Membranes for High-Flux Separation of Dyes from Water

Li, Zhan ; Das, Saikat ; Sekine, Taishu ; Mabuchi, Haruna ; Kaneko, Ryo ; Sakai, Jin ; Irie, Tsukasa ; Kamio, Eiji ; Yoshioka, Tomohisa ; Suo,…

(Citation)
ACS Applied Nano Materials,5(12):17632-17639

(Issue Date)
2022-12-23

(Resource Type)
journal article

(Version)
Version of Record

ACS APPLIED NANO MATERIALS

www.acsanm.org Article

Control over the Hydrophilicity in the Pores of Covalent Organic Framework Membranes for High-Flux Separation of Dyes from Water

Zhan Li,[#] Saikat Das,[*,#] Taishu Sekine, Haruna Mabuchi, Ryo Kaneko, Jin Sakai, Tsukasa Irie, Eiji Kamio, Tomohisa Yoshioka, Jinquan Suo, Qianrong Fang, Tokuhisa Kawawaki, Hideto Matsuyama,[*] and Yuichi Negishi[*]

Cite This: *ACS Appl. Nano Mater.* 2022, 5, 17632−17639 Read Online

ACCESS | Metrics & More | Article Recommendations | Supporting Information

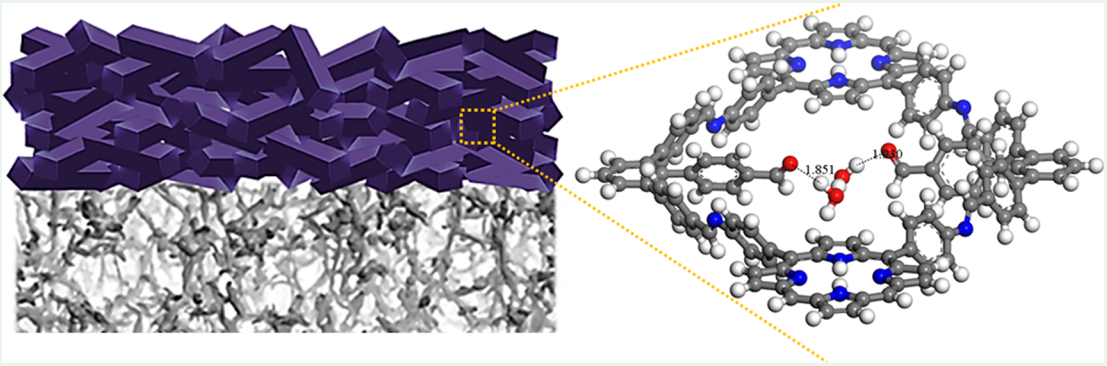

ABSTRACT: Membrane separation is making substantial contributions to water purification. Particularly important is the pore-size control designed for molecular sieving. Regarding water permeation, filtration experiments accentuate the importance of hydrophilic pores in enhancing the water adsorption capacity, while hydrophobic pores enable low-friction water diffusion. To reach both the criteria, we herein precisely design the pore metrics and pore functionalities to prepare a covalent organic framework (COF), termed TUS-46, membrane. Credited with pore sizes befitting for size-selective molecular exclusion and negative electrostatic pore walls, the TUS-46 COF membrane shows excellent rejection performance toward anionic dyes. Attributed to the free aldehyde functionalities in the framework resulting from unbalanced stoichiometry, the TUS-46 COF membrane also shows a 10-fold higher water permeance compared to the analogue COF membrane without free aldehyde functionalities. In particular, the in situ construction of hydrophilic nanospaces partaking in high water uptake and hydrophobic nanospaces facilitating fast water diffusion in a single COF structure endows the TUS-46 membranes with unprecedentedly high water flux. The stoichiometric imbalance approach presented herein offers a different route to COF membrane fabrication and may impart with an unprecedented control handle on the permeability and separation selectivity of COF membranes.

KEYWORDS: *covalent organic framework, membrane, hydrophilic, water treatment, dye separation*

INTRODUCTION

Water was at the forefront in the development of all early civilizations such as Mesopotamia (Tigris and Euphrates rivers), Egypt (Nile river), Indus valley civilization (Indus river), and China (Yellow river).[1] Cut to the present, the Yangtze and Pearl River basins accounted for over one-half of the sudden water pollution incidents in China from 2006 to 2018, largely relating to discharge of pollutants from industries.[2] The textile industry alone utilized 79 billion cubic meters of water worldwide in 2015 and that textile manufacturing accounted for approximately 20% of clean water pollution resulting from dyeing and finishing.[3] A substantial share amounting to 10−60% of dyes is lost in the course of textile finishing, entailing a waste of 280,000 t of dyes annually.[4] The dyes in industrial effluents can have perilous effects on aquatic species and human health.

Membranes hold significant potential for water treatment, attributed to their high separation selectivity, small footprint, cost and energy efficiency, and scalability.[5] The core advantage

Received: August 2, 2022
Accepted: September 12, 2022
Published: September 26, 2022

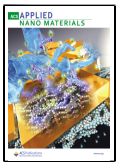

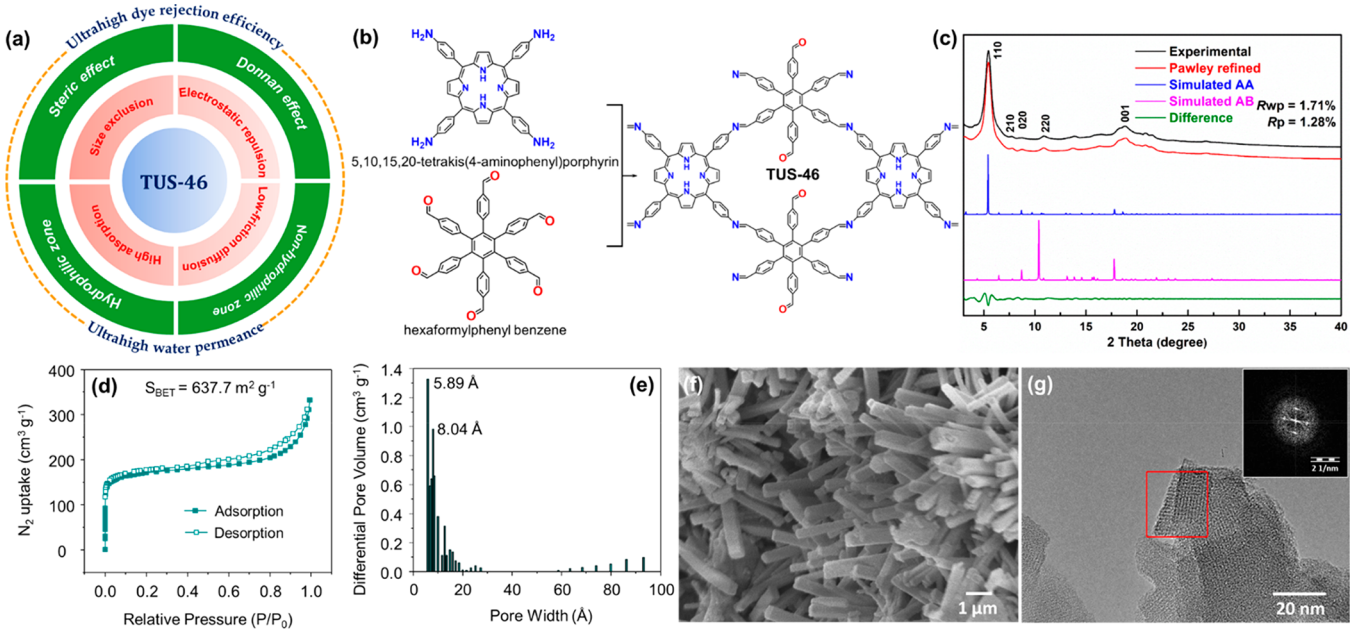

Figure 1. (a) TUS-46 COF membrane exemplifies "high dye rejection" attributed to its size- and charge-selective molecular sieving as well as "high water permeance" attributed to its high-adsorption hydrophilic pores and low-friction hydrophobic pores. (b) Chemical structure of TUS-46 COF. (c) XRD patterns of TUS-46. (d) Nitrogen sorption isotherms of TUS-46. (e) Pore size distribution profile of TUS-46. (f) SEM image of TUS-46. (g) HRTEM image of TUS-46. Inside is the fast Fourier transform (FFT) pattern acquired from the area enclosed by the red box.

of polymeric membranes is its processability and excellent mechanical properties.[6] Nevertheless, membrane fouling and the permeability−selectivity trade-off are some of the critical challenges hindering the adoption of polymer membranes in water purification.[6,7] Graphene oxide (GO) membranes are interesting platforms for wastewater reclamation owing to their tunable molecular sieving by adjusting the interlayer spacing in GO laminates, easy dispersibility of GO sheets and their inclusion in polymer matrices, and their oxygen-rich functional groups enabling the preparation of GO-based composites.[8−10] However, the shortcoming is the low water flux owing to the (a) dearth of sp^2 domains of pristine graphene and (b) oxygen-rich functional groups obstructing the space for water passage by the formation of hydrogen bonding.[11] Metal−organic framework (MOF) membranes have recently aroused great interest in separation applications owing to their high surface areas providing ample adsorption sites for guests, precise control over pore metrics, and easily functionalizable pore walls.[12−14] However, inadequate hydrolytic stability of some MOF membranes is a potential bottleneck for water purification.[14] The allure of covalent organic framework (COF) membranes stems from their internal surface area with a well-defined pore structure yielding high selectivity as well as permeability, good thermochemical stabilities imparted by strong covalent linkages, and tailored functionalities realized by customizing the organic building blocks.[15,16]

Inspired by the successful preparation of sub-stoichiometric COFs,[17,18] we herein report the fabrication of a novel porphyrinic TUS-46 COF membrane via a stoichiometric imbalance approach. The tetratopic porphyrin building block was judiciously chosen for its aromatic character that would compose the hydrophobic domains of the COF framework. On the other hand, the hexagonal aldehyde building block was selected to conceive the hydrophilic domains of the COF framework emanating from the unreacted aldehyde functionalities after reticulation. The hydrophilic domains enhancing the adsorption of water molecules and hydrophobic domains facilitating fast water diffusion impart the TUS-46 membranes with outstanding water flux. Besides, the synergy of molecular sieving and electrostatic repulsion renders a superlative dye rejection performance (Figure 1a).

EXPERIMENTAL SECTION

Synthesis of TUS-46. A Pyrex tube (body length = 14.5 cm, neck length = 9 cm, volume 10 mL) was charged with hexaformylphenyl benzene (HFPB, 35.14 mg, 0.05 mmol), 5,10,15,20-tetrakis(4-aminophenyl)porphyrin (TAPP, 50.61 mg, 0.075 mmol), anhydrous *n*-butanol (1 mL), and 6 M aqueous acetic acid (0.1 mL). The mixture was sonicated for 15 min in an ultrasonic bath to produce a homogenous dispersion. The Pyrex tube was degassed by three freeze−pump−thaw cycles and subsequently flame-sealed. The sealed tube was kept at RT for 4 h, followed by 120 °C for 3 days. A dark purple precipitate was isolated by centrifugation and washed with tetrahydrofuran (THF, 5 mL × 5 times). The resulting solid was dried at room temperature and further purified by Soxhlet extraction with THF (24 h). After being activated under dynamic vacuum at 100 °C for 5 h, the dark purple powder of TUS-46 COF (22.90 mg) was obtained. Anal. Calcd. for $[C_{92}H_{54}N_8O_2]_n$: C: 85.22; H: 4.06; N: 8.12; O: 2.61. Found: C: 81.50; H: 3.70; N: 8.98; O: 5.81.

Fabrication of TUS-46 Membranes. Polyvinylidene difluoride (PVDF) substrates of diameter 2 cm were immersed in 7.5 M NaOH aqueous solution at 80 °C for 3 h to activate the hydroxyl groups on the substrate surface. Then, the substrates were repeatedly washed with distilled water until a neutral condition was obtained and later dried. After this, the substrates were treated with 1.5% (3-aminopropyl)triethoxysilane (APTES) in ethanol for 1 h to obtain amine groups-functionalized substrate surface. HFPB (35.14 mg, 0.05 mmol) and TAPP (50.61 mg, 0.075 mmol) were weighed, ground together with a mortar and pestle, and introduced in a Teflon-lined autoclave reactor. The mixture was dissolved in anhydrous *n*-butanol (1 mL). The PVDF substrate was placed horizontally with the amine groups-functionalized surface face up inside the reactor. 6 M aqueous acetic acid (0.1 mL) was added dropwise in the autoclave reactor, followed by heating the reactor at 120 °C for 3 days. The resulting

https://doi.org/10.1021/acsanm.2c03392
ACS Appl. Nano Mater. 2022, 5, 17632−17639

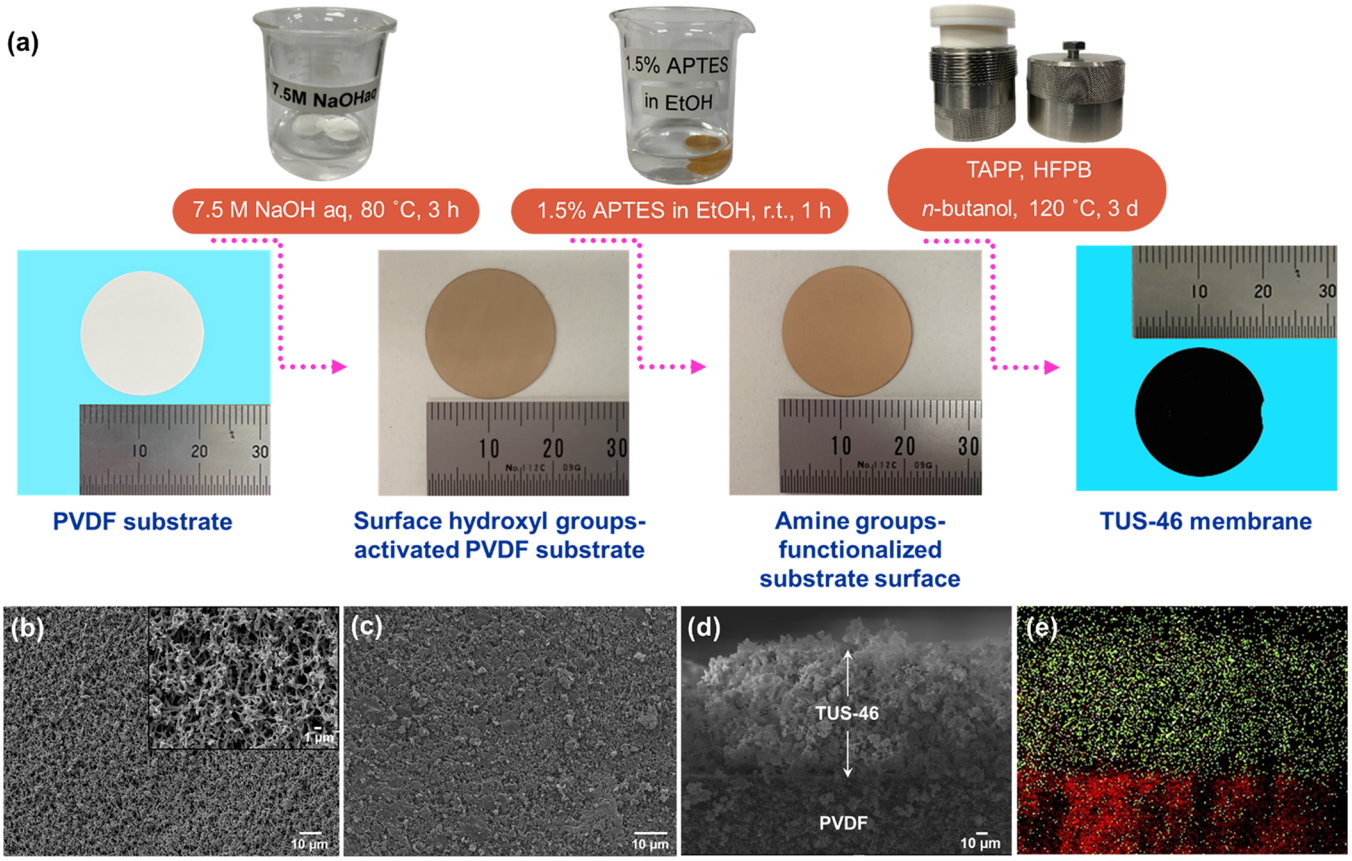

Figure 2. (a) Fabrication method for TUS-46 membranes. SEM top view of the (b) PVDF substrate and (c) TUS-46 membrane. (d) SEM cross-sectional view of the COF layer and PVDF substrate layer in the TUS-46 membrane and (e) energy-dispersive X-ray spectroscopy (EDX) elemental mapping image of nitrogen (yellow) and fluorine (red).

membrane was washed with THF and dried in air at room temperature.

Dye Separation Tests of TUS-46 Membranes. The dye separation performance of the bare substrate and COF membranes was evaluated on a home-built system. Two silicon sheets (diameter = 2.0 cm) with a hole (diameter = 1.0 cm) in the center were attached to both sides of the membranes. The silicon sheet-covered membranes were then fixed into a customized membrane cell and sealed on the edge by an O-ring. 150 ppm of the dye aqueous solution was fed into one side of the membrane by a peristaltic pump at a flow rate of 10 mL/min. The pressure at the feed side was controlled by a back pressure regulator. The amount of the permeated liquid was measured by a mass balance (FX-3000i WP; A&D Co., Ltd., Tokyo, Japan). The residual dye concentration in the permeated liquid was determined by a UV−Vis spectrophotometer (V-650, JASCO Co., Tokyo, Japan).

The permeance of the membrane P (LMH bar^{-1}) can be calculated by

$$P = \frac{V}{t \times A \times p}$$

where V is the volume (L) of liquid permeated through the membrane during time period of t (hours), A is the membrane area (m^2), and p (bar) is the pressure on the feed side of the membrane.

The dye rejection ratio is defined as

$$R = \left(1 - \frac{R_p}{R_f}\right) \times 100\%$$

where R_p and R_f represent the dye concentrations in the permeate and feed side, respectively.

RESULTS AND DISCUSSION

TUS-46 COF was prepared by the acid-catalyzed Schiff-base condensation reaction of HFPB and TAPP under solvothermal conditions (Figure 1b). The crystal structure of TUS-46 was solved from powder X-ray diffraction (PXRD) complemented with structural simulations using the Materials Studio[19] software suite. As shown in Figure 1c, the PXRD pattern of TUS-46 reveals pronounced peaks at 2θ = 5.45, 7.63, 8.70, 10.90, and 18.79°, which were assigned to the (110), (210), (020), (220), and (001) facets, respectively. Pawley refinement of the experimental PXRD pattern was accomplished furnishing unit-cell parameters a = 27.2907 Å, b = 20.3587 Å, c = 4.9848 Å, $\alpha = \beta = \gamma$ = 90°, and low residual factors R_{wp} = 1.71%, R_p = 1.28%. The Pawley refined PXRD pattern (red curve, Figure 1c) matches well with the experimental PXRD pattern (black curve, Figure 1c), which is reflected from the minor difference plot (green curve, Figure 1c). Structural modeling was performed with **sql** topology in the $P1$ space group. The calculated XRD pattern of TUS-46 corresponding to eclipsed AA stacking matches with the PXRD pattern, while that corresponding to staggered AB stacking differs from the PXRD pattern (Figure 1c and Figures S16 and S17). N_2 gas physisorption measurements of TUS-46 carried out at 77 K show a type I isotherm revealing the microporous nature of the COF (Figure 1d). A minor hysteresis loop can be observed over $0.4 < P/P_0 < 0.6$ that can be attributed to mesopores arising out of stacking faults in 2D COFs.[20] Application of the Brunauer−Emmett−Teller (BET) model over the relative pressure range of 0.01−0.1 gave a specific surface area of 637.7

https://doi.org/10.1021/acsanm.2c03392
ACS Appl. Nano Mater. 2022, 5, 17632−17639

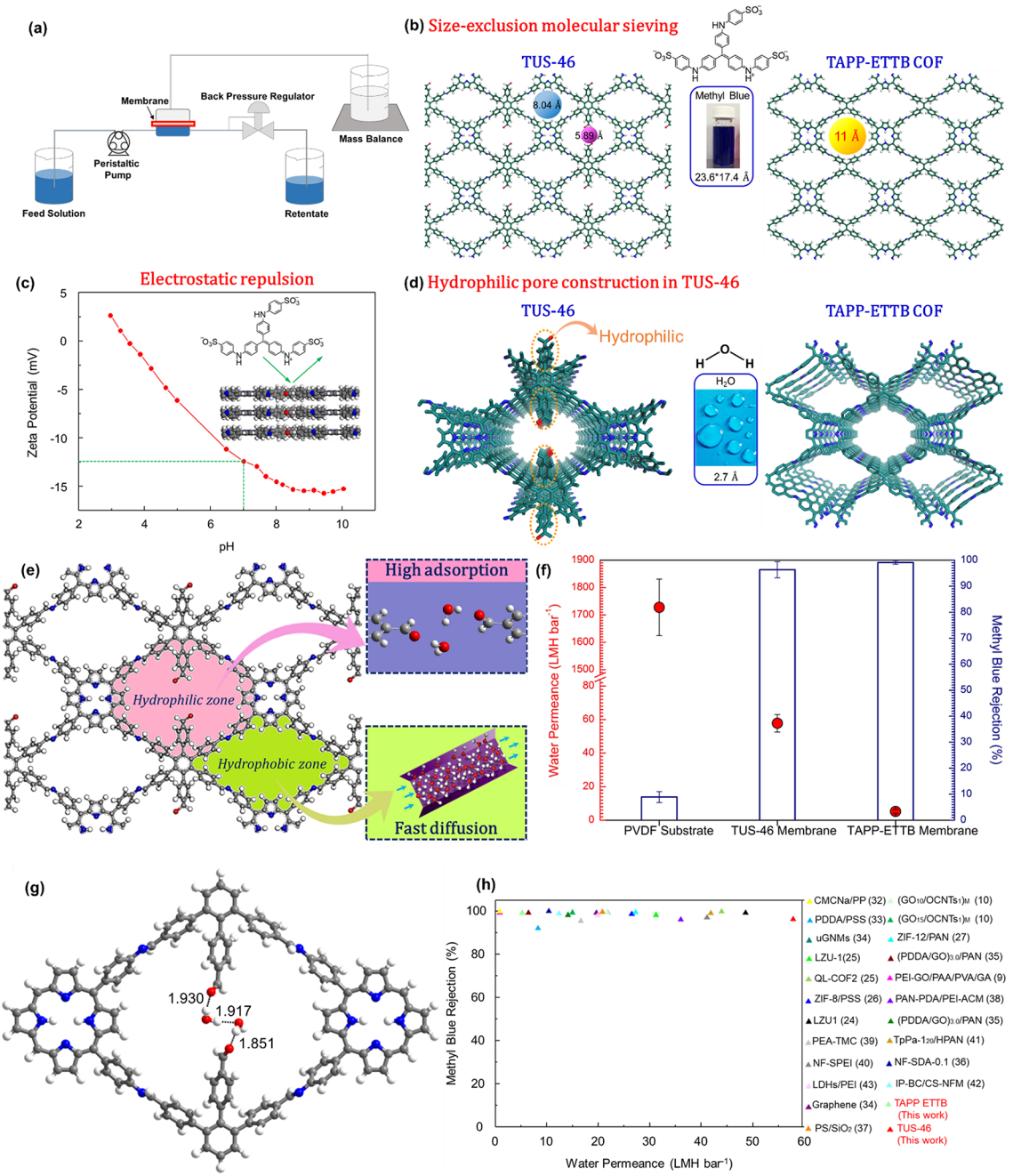

Figure 3. (a) Schematic diagram of the experimental setup for dye removal from aqueous solution. (b) Molecular sieving effect of the TUS-46 and TAPP-ETTB COF membranes on MB rejection (C: cyan, H: white, N: blue, O: red). (c) Zeta potential of the TUS-46 membrane at different pH conditions. (d) The bare aldehyde groups adorning the channel space in the TUS-46 membranes contribute to their enhanced water permeance. (e) Coexistence of hydrophilic and non-hydrophilic zones in the TUS-46 membrane with the hydrophilic zones assisting in high water adsorption and non-hydrophilic zones in fast water diffusion (C: gray, H: white, N: blue, O: red). (f) Water permeance and MB rejection of the PVDF substrate, TUS-46 membrane, and TAPP-ETTB membrane. (g) DFT optimized trimer structure. The dash lines and the numbers on them are the hydrogen bonding interaction distances in angstrom. (h) Comparative analysis of the MB rejection performance of the TUS-46 and TAPP-ETTB COF membranes against current state-of-the art membranes. The numbers in parentheses indicate the references.

$m^2\ g^{-1}$ (Figure S15). To obtain the pore size distribution of TUS-46, the nonlocal density functional theory (NLDFT) with a slit pore model for N_2 adsorption at 77 K on carbon and a method of non-negative regularization was used. The pore sizes of TUS-46 were derived as 5.89 and 8.04 Å (Figure 1e). The Fourier-transform infrared (FT-IR) spectra of the HFPB and TAPP building blocks show the C═O (1702 cm^{-1}) and N−H (3443 cm^{-1}) stretching of aldehydes and amines, respectively. The attenuation of the amino N−H stretching and the emergence of the new imine C═N stretching band at 1621 cm^{-1} in the FT-IR spectrum of TUS-46 testify to the successful construction of the imine COF. Besides, the peak at 1697 cm^{-1} corresponds to the C═O stretching of residual aldehydes in TUS-46 (Figure S6). The solid-state ^{13}C cross-polarization magic angle spinning (CP/MAS) NMR spectrum of TUS-46 reaffirmed the presence of imine linkages by the peak appearing at 158 ppm (Figure S5). Scanning electron microscopy (SEM) inspection presented the rod-like morphol-

https://doi.org/10.1021/acsanm.2c03392
ACS Appl. Nano Mater. 2022, 5, 17632−17639

ogy of TUS-46 crystals (Figure 1f and Figure S7a). The lattice fringes could be observed in high-resolution transmission electron microscopy (HRTEM) imaging (Figure 1g and Figure S10). According to the thermogravimetric analysis (TGA), high thermal stability up to 435 °C with a 5% weight loss was observed for TUS-46 (Figure S11). Moreover, TUS-46 exhibited high chemical stability after treatment with a variety of organic solvents, water, and aqueous HCl and NaOH solutions, as evident from its retention of crystallinity in the PXRD profiles (Figure S12).

In this study, PVDF was adopted as the support of the COF membrane. PVDF was chosen owing to its (a) unprecedented chemical resistance coming from the strong C−C and C−F bonds and (b) good thermal stability attributed to its crystalline phase and mechanical flexibility attributed to its amorphous phase.[21,22] The SEM top view of the PVDF membrane reveals an interconnected porous structure (Figure 2b). The thickness of the PVDF membrane was ∼90 μm (Figure S8a). On the downside, however, the PVDF membrane is inherently hydrophobic, which increases the likelihood of membrane fouling, and has a high shrinkage ratio.[22] This calls for the surface engineering of the PVDF membrane. In the first step, the PVDF substrate was subjected to hydroxylation as provision for bonding between the −OH groups and ethoxy groups of APTES in the second step. As can be seen in Figure 2a, the color of the PVDF substrates changed from white to pale brown after hydroxylation. The APTES modification of the PVDF membrane can render amino groups on the surface, improving the compatibility between the COF layer and PVDF support by strong chemical bonding.[23] Digital photographs of the PVDF substrate and TUS-46 membrane shown in Figure 2a reveal uniform coverage of the white PVDF surface by a dark-purple COF layer. As seen in Figure S18, the XRD pattern of the TUS-46 membrane matches well with the PXRD pattern of the TUS-46 powder, validating the phase purity of the top COF layer. The TUS-46 membrane surface and cross section was observed using SEM. Surface observation showed the formation of a continuous and compact COF layer (Figure 2c). Cross-section observation with a related EDX map (Figure 2d,e and Figure S8b) of the TUS-46 membrane identifies the COF and PVDF layers, each of thickness ∼90 μm. The wetting behavior of the pristine PVDF substrate and TUS-46 membrane was probed by contact angle measurements. The water contact angle of the PVDF substrate is 138° and decreases to 137° after 1 min, reflecting the hydrophobicity of PVDF. After the growth of the COF layer, the membrane showed a low water contact angle of 56° and that drastically reduced to 9° in 1 min, suggesting enhanced hydrophilicity of the membrane surface (Figure S19).

Next, we investigated the dye rejection performance of the TUS-46 membrane from aqueous solutions. All dye rejection tests were performed in a dead-end configuration at 20−22 °C. Figure 3a illustrates the schematic of the experimental setup for dye removal from aqueous solution. The PVDF substrates showed 8.9% rejection to methyl blue (MB) and 1727.7 LMH bar^{-1} water permeance. This is because its pores are too large (0.1 μm) to hinder molecular transport. Intriguingly, the construction of the TUS-46 membrane on the PVDF substrate results in significantly higher MB dye rejection (96.3%) than that of the control substrate (Figure 3f), attributed to the (a) COF crystals covering the pores on the PVDF surface and (b) COF pore apertures (5.89 Å, 8.04 Å) with molecular sieving characteristics discriminating MB (23.6 × 17.4 Å)[23] from water (2.7 Å) molecules (Figure 3b). The zeta potential of the TUS-46 membrane was also investigated at different pH conditions to understand the effect of surface charge in MB dye rejection. As shown in Figure 3c, the zeta potential of the TUS-46 membrane was found to be −12.4 mV at pH 7. Hence, the electrostatic repulsion between the negatively charged COF membrane surface and anionic MB dye (Donnan effect[16]) also plays a contributory role in the dye rejection performance of the TUS-46 membrane. A water permeance as high as 57.8 LMH bar^{-1} was achieved (Figure 3f), which surpasses the water permeances for MB separation by most COF (LZU1: 48.5 LMH bar^{-1}; QL-COF2: 43.9 LMH bar^{-1})[24,25] and MOF (ZIF-8/PSS: 26.5 LMH bar^{-1}; ZIF-11/PAN: 46.4 LMH bar^{-1}; ZIF-12/PAN: 27.2 LMH bar^{-1})[26,27] membranes with dye rejection rate >95% yet reported. In this contribution, we address the intrinsic hydrophilicity of TUS-46 membranes through direct reticular construction, unlike many other previous reports. The alumina tube-supported COF-LZU1 membrane reported by Caro et al.[24] owes mostly its hydrophilicity to the substrate material, considering that COF-LZU1 has a highly aromatic structure and that the nonpolar C−C and C−H bonds that make up the aromatic rings are water-insoluble. In another example, the hydrophilicity of the ZIF-8/PSS nanofiltration membrane prepared by Li et al.[26] derives from the PSS polymer matrix, since ZIF-8 is inherently hydrophobic. In a separate contribution, Huang and co-workers prepared a IISERP-COOH-COF1 membrane with enhanced hydrophilicity through post-synthetic modification.[28] In the present study, the ultrahigh water flux of the TUS-46 membrane stems from the direct concomitant construction of hydrophilic and hydrophobic domains in a single framework (Figure 3e). The pore channels (5.89 Å) adorned with residual aldehyde functionalities serve as hydrophilic nanospaces wherein the aldehyde moieties with high adsorption enthalpy facilitate water adsorption (wetting[29]). On the other hand, the 8.04 Å pore channels exemplify hydrophobic nanospaces performing the function of low-friction rapid diffusion pathways for water owing to the weak interaction of these hydrophobic nanospaces with water molecules. This technique of accommodating philic as well as non-philic domains has been applied to GO membranes for enhanced CO_2 permeance.[30] We have imbibed this concept in the design and fabrication of TUS-46 COF membranes.

To probe the role of the residual aldehyde groups in enhancing the water permeance of the TUS-46 membranes, we fabricated analogue TAPP-ETTB COF[31] membranes without residual aldehyde functionalities and tested their MB separation performance from aqueous solutions. Cross-sectional SEM image with corresponding EDX map (Figure S9) of the TAPP-ETTB COF membrane indicates the successful growth of a continuous and uniform layer of TAPP-ETTB COF atop the PVDF substrate. The thickness of the TAPP-ETTB COF layer was found to be ∼90 μm, comparable to that of the TUS-46 layer. With pore size (11 Å) smaller than the size of the MB molecule (Figure 3b), the TAPP-ETTB COF membrane led to a 99.1% rejection of MB (Figure 3f). However, an appreciably lower water permeance of 5.2 LMH bar^{-1} (Figure 3f) was obtained owing to the hydrophobic character of TAPP-ETTB COF (Figure 3d). A comparative analysis of the MB rejection performance of the TUS-46 and TAPP-ETTB COF membranes against current state-of-the art membranes is provided in Figure 3h.[9,10,24−27,31−43] The XRD investigation after dye removal tests validated the retention of

https://doi.org/10.1021/acsanm.2c03392
ACS Appl. Nano Mater. 2022, 5, 17632−17639

the crystallinity of TUS-46 membranes (Figure S18), with no changes in the crystal structure or morphology detected by SEM (Figure S7b). Besides, the long-term hydrolytic stability of TUS-46 could be substantiated from the preservation of crystallinity and chemical makeup after immersing in water over 4 weeks, as evident from the XRD profiles (Figure S13) and FT-IR spectra (Figure S14), respectively.

To further our understanding of the high water flux of TUS-46, the hydrogen bonding interactions between water molecules and the COF fragment were investigated using density functional theory (DFT) simulation. First, we built the structure of the COF using the Materials Studio software package and further optimized it using the Gaussian plane-wave computational package CP2K 8.1 program at the PBE-D3/DZVP-MOLOPT-SR-GTH level.[44−51] Grimme's dispersion correction (D3) was included to interpret the weak interactions. The convergence cutoff was set to 400 eV, and largest forces on the atoms were less than 0.00045 hartree/bohr. Then, we built a macrocycle fragment to represent the channel environment of the COF and put two water molecules between the two free aldehyde groups. In order to better realize the configuration of the fragment in the bulk material, all atoms except hydrogen atoms, water molecules, and aldehyde groups were set to be fixed. The macrocycle fragment was obtained from the DFT-optimized structure and saturated with hydrogen atoms. The constraint optimization of the hydrogen-saturated fragment and the trimer was carried using the ORCA program at the BLYP-D3/def2-TZVP level with an SMD model of water.[52−55] As shown in the DFT-optimized trimer structure (Figure 3g), there formed strong hydrogen bonds between water molecules and the free aldehyde groups, illustrating the hydrophilicity of the channel. After geometry optimization, the O−H···O═C hydrogen bonding distances between water molecules and free aldehyde groups are 1.930 and 1.851 Å, respectively, which is indicative of a strong interaction between the fragment and water molecules, as well as hydrophilicity of the pore surface.

CONCLUSIONS

This study describes the in situ growth of imine-based 2D TUS-46 COF membranes on PVDF substrates for rapid and highly selective removal of dyes from aqueous solutions. The COF membranes exhibited significant rejection of 96.3% to MB dye, which is far higher than that of pristine PVDF substrates. The ordered 1D nanochannels and unreacted aldehyde functionalities appearing from unbalanced stoichiometry in TUS-46 membranes endow them with high water permeance of 57.8 LMH bar^{-1}, which is 10 times higher than that of analogue TAPP-ETTB COF membranes without residual aldehyde functionalities. This stoichiometric imbalance approach applied to COF membrane fabrication enables periodically crafted hydrophilic and hydrophobic COF pore environments through one-pot reticular construction as distinguished from post-synthetic channel engineering or relying on the hydrophilicity of the substrates/composite matrices.

ASSOCIATED CONTENT

Supporting Information

The Supporting Information is available free of charge at https://pubs.acs.org/doi/10.1021/acsanm.2c03392.

^{13}C CP/MAS NMR spectrum, FT-IR spectra, SEM and TEM images, TGA trace, structure simulations, crystallographic information, wettability, and nanofiltration performance (PDF)

AUTHOR INFORMATION

Corresponding Authors

Saikat Das − *Department of Applied Chemistry, Faculty of Science, Tokyo University of Science, Tokyo 162-8601, Japan*; Email: saikatdas@rs.tus.ac.jp

Hideto Matsuyama − *Research Center for Membrane and Film Technology, Department of Chemical Science and Engineering, Kobe University, Kobe 657-8501, Japan*; orcid.org/0000-0003-2468-4905; Email: matuyama@kobe-u.ac.jp

Yuichi Negishi − *Department of Applied Chemistry, Faculty of Science, Tokyo University of Science, Tokyo 162-8601, Japan*; orcid.org/0000-0003-3965-1399; Email: negishi@rs.tus.ac.jp

Authors

Zhan Li − *Research Center for Membrane and Film Technology, Department of Chemical Science and Engineering, Kobe University, Kobe 657-8501, Japan*

Taishu Sekine − *Department of Applied Chemistry, Faculty of Science, Tokyo University of Science, Tokyo 162-8601, Japan*

Haruna Mabuchi − *Department of Applied Chemistry, Faculty of Science, Tokyo University of Science, Tokyo 162-8601, Japan*

Ryo Kaneko − *Department of Applied Chemistry, Faculty of Science, Tokyo University of Science, Tokyo 162-8601, Japan*

Jin Sakai − *Department of Applied Chemistry, Faculty of Science, Tokyo University of Science, Tokyo 162-8601, Japan*

Tsukasa Irie − *Department of Applied Chemistry, Faculty of Science, Tokyo University of Science, Tokyo 162-8601, Japan*

Eiji Kamio − *Research Center for Membrane and Film Technology, Department of Chemical Science and Engineering, Kobe University, Kobe 657-8501, Japan*; orcid.org/0000-0002-1331-0871

Tomohisa Yoshioka − *Research Center for Membrane and Film Technology, Department of Chemical Science and Engineering, Kobe University, Kobe 657-8501, Japan*; orcid.org/0000-0002-7489-441X

Jinquan Suo − *State Key Laboratory of Inorganic Synthesis and Preparative Chemistry, Jilin University, Changchun 130012, China*

Qianrong Fang − *State Key Laboratory of Inorganic Synthesis and Preparative Chemistry, Jilin University, Changchun 130012, China*; orcid.org/0000-0003-3365-5508

Tokuhisa Kawawaki − *Department of Applied Chemistry, Faculty of Science, Tokyo University of Science, Tokyo 162-8601, Japan*; orcid.org/0000-0003-3282-8964

Complete contact information is available at: https://pubs.acs.org/10.1021/acsanm.2c03392

Author Contributions

[#]Z.L. and S.D. contributed equally to this work.

Author Contributions

The manuscript was written through contributions of all authors. All authors have given approval to the final version of the manuscript.

https://doi.org/10.1021/acsanm.2c03392
ACS Appl. Nano Mater. 2022, 5, 17632−17639

Notes

The authors declare no competing financial interest.

■ ACKNOWLEDGMENTS

This work was supported by the Japan Society for the Promotion of Science (JSPS) KAKENHI (grant numbers 20H02698 and 20H02552), Scientific Research on Innovative Areas "Innovations for Light-Energy Conversion" (grant numbers 18H05178 and 20H05115), Scientific Research on Innovative Areas "Hydrogenomics" (grant number 21H00027), Scientific Research on Innovative Areas "Aquatic Functional Materials" (grant numbers 18H05178 and 22H04562), and JST Adaptable and Seamless Technology Transfer Program through Target-driven R&D (A-STEP, grant number JPMJTM20MS). Funding provided by the Yazaki Memorial Foundation for Science and Technology, the Ogasawara Foundation for the Promotion of Science and Engineering, the Kao Foundation for Arts and Sciences, and TEPCO Memorial Foundation, the Japan Science Society, the Takahashi Industrial and Economic Research Foundation, and Kobe University Strategic International Collaborative Research Grant (Type B Fostering Joint Research), and the Kubota Corporation is also gratefully acknowledged.

■ REFERENCES

(1) *Key Components of Civilization*; https://education.nationalgeographic.org/resource/key-components-civilization

(2) Xu, J.; Xu, M.; Zhao, Y.; Wang, S.; Tao, M.; Wang, Y. Spatial-temporal distribution and evolutionary characteristics of water environment sudden pollution incidents in China from 2006 to 2018. *Sci. Total Environ.* **2021**, *801*, No. 149677.

(3) *The impact of textile production and waste on the environment (infographic)*; https://www.europarl.europa.eu/news/en/headlines/society/20201208STO93327/the-impact-of-textile-production-and-waste-on-the-environment-infographic#:~:text=Textile%20production%20is%20estimated%20to,into%20the%20ocean%20a%20year.

(4) Berradi, M.; Hsissou, R.; Khudhair, M.; Assouag, M.; Cherkaoui, O.; El Bachiri, A.; El Harfi, A. Textile finishing dyes and their impact on aquatic environs. *Heliyon* **2019**, *5*, No. e02711.

(5) Kuvarega, A. T.; Mamba, B. B. Photocatalytic Membranes for Efficient Water Treatment. In *Semiconductor Photocatalysis - Materials, Mechanisms and Applications*; Cao, W., Eds.; IntechOpen: London, United Kingdom, 2016.

(6) Kumar, R.; Ismail, A. F. Fouling control on microfiltration/ultrafiltration membranes: Effects of morphology, hydrophilicity, and charge. *J. Appl. Polym. Sci.* **2015**, *132*, 42042−45749.

(7) Moon, J. D.; Freeman, B. D.; Hawker, C. J.; Segalman, R. A. Can Self-Assembly Address the Permeability/Selectivity Trade-Offs in Polymer Membranes? *Macromolecules* **2020**, *53*, 5649−5654.

(8) Kang, X.; Cheng, Y.; Wen, Y.; Qi, J.; Li, X. Bio-inspired co-deposited preparation of GO composite loose nanofiltration membrane for dye contaminated wastewater sustainable treatment. *J. Hazard. Mater.* **2020**, *400*, No. 123121.

(9) Wang, N.; Ji, S.; Zhang, G.; Li, J.; Wang, L. Self-assembly of graphene oxide and polyelectrolyte complex nanohybrid membranes for nanofiltration and pervaporation. *Chem. Eng. J.* **2012**, *213*, 318−329.

(10) Kang, H.; Shi, J.; Liu, L.; Shan, M.; Xu, Z.; Li, N.; Li, J.; Lv, H.; Qian, X.; Zhao, L. Sandwich morphology and superior dye-removal performances for nanofiltration membranes self-assemblied via graphene oxide and carbon nanotubes. *Appl. Surf. Sci.* **2018**, *428*, 990−999.

(11) Zhang, Q.; Qian, X.; Thebo, K. H.; Cheng, H.-M.; Ren, W. Controlling reduction degree of graphene oxide membranes for improved water permeance. *Sci. Bull.* **2018**, *63*, 788−794.

(12) Kadhom, M.; Deng, B. Metal-organic frameworks (MOFs) in water filtration membranes for desalination and other applications. *Appl. Mater. Today* **2018**, *11*, 219−230.

(13) Jun, B.-M.; Al-Hamadani, Y. A. J.; Son, A.; Park, C. M.; Jang, M.; Jang, A.; Kim, N. C.; Yoon, Y. Applications of metal-organic framework based membranes in water purification: A review. *Sep. Purif. Technol.* **2020**, *247*, No. 116947.

(14) Zhang, M.-Y.; Wang, X.-P.; Lin, R.; Liu, Y.; Chen, F.-S.; Cui, L.-S.; Meng, X.-M.; Hou, J. Improving the hydrostability of ZIF-8 membrane by biomolecule towards enhanced nanofiltration performance for dye removal. *J. Membr. Sci.* **2021**, *618*, No. 118630.

(15) Yuan, S.; Li, X.; Zhu, J.; Zhang, G.; Van Puyvelde, P.; Van der Bruggen, B. Covalent organic frameworks for membrane separation. *Chem. Soc. Rev.* **2019**, *48*, 2665−2681.

(16) Zhang, S.; Zhao, S.; Jing, X.; Niu, Z.; Feng, X. Covalent organic framework-based membranes for liquid separation. *Org. Chem. Front.* **2021**, *8*, 3943−3967.

(17) Banerjee, T.; Haase, F.; Trenker, S.; Biswal, B. P.; Savasci, G.; Duppel, V.; Moudrakovski, I.; Ochsenfeld, C.; Lotsch, B. V. Sub-stoichiometric 2D covalent organic frameworks from tri- and tetratopic linkers. *Nat. Commun.* **2019**, *10*, 2689.

(18) Chen, L.; Gong, C.; Wang, X.; Dai, F.; Huang, M.; Wu, X.; Lu, C.-Z.; Peng, Y. Substoichiometric 3D Covalent Organic Frameworks Based on Hexagonal Linkers. *J. Am. Chem. Soc.* **2021**, *143*, 10243−10249.

(19) *Materials Studio* ver. 7.0; Accelrys Inc.: San Diego, CA.

(20) Li, X.; Gao, Q.; Aneesh, J.; Xu, H.-S.; Chen, Z.; Tang, W.; Liu, C.; Shi, X.; Adarsh, K. V.; Lu, Y.; Loh, K. P. Molecular Engineering of Bandgaps in Covalent Organic Frameworks. *Chem. Mater.* **2018**, *30*, 5743−5749.

(21) Düputell, D.; Staude, E. Heterogeneous modification of ultrafiltration membranes made from poly (vinylidene fluoride) and their characterization. *J. Membr. Sci.* **1993**, *78*, 45−51.

(22) Wu, L.; Sun, J.; Wang, Q. Poly(vinylidene fluoride)/polyethersulfone blend membranes: Effects of solvent sort, polyethersulfone and polyvinylpyrrolidone concentration on their properties and morphology. *J. Membr. Sci.* **2006**, *285*, 290−298.

(23) Lu, K. J.; Zuo, J.; Chang, J.; Kuan, H. N.; Chung, T. S. Omniphobic Hollow-Fiber Membranes for Vacuum Membrane Distillation. *Environ. Sci. Technol.* **2018**, *52*, 4472−4480.

(24) Fan, H.; Gu, J.; Meng, H.; Knebel, A.; Caro, J. High-Flux Membranes Based on the Covalent Organic Framework COF-LZU1 for Selective Dye Separation by Nanofiltration. *Angew. Chem., Int. Ed.* **2018**, *57*, 4083−4087.

(25) Yang, Y.; Yu, L.; Chu, T.; Niu, H.; Wang, J.; Cai, Y. Constructing chemical stable 4-carboxyl-quinoline linked covalent organic frameworks via Doebner reaction for nanofiltration. *Nat. Commun.* **2022**, *13*, 2615.

(26) Zhang, R.; Ji, S.; Wang, N.; Wang, L.; Zhang, G.; Li, J. R. Coordination-Driven In Situ Self-Assembly Strategy for the Preparation of Metal−Organic Framework Hybrid Membranes. *Angew. Chem., Int. Ed.* **2014**, *53*, 9775−9779.

(27) Wang, N.; Li, X.; Wang, L.; Zhang, L.; Zhang, G.; Ji, S. Nanoconfined Zeolitic Imidazolate Framework Membranes with Composite Layers of Nearly Zero Thickness. *ACS Appl. Mater. Interfaces* **2016**, *8*, 21979−21983.

(28) Liu, C.; Jiang, Y.; Nalaparaju, A.; Jiang, J.; Huang, A. Post-synthesis of a covalent organic framework nanofiltration membrane for highly efficient water treatment. *J. Mater. Chem. A* **2019**, *7*, 24205−24210.

(29) Xu, F.; Wei, M.; Zhang, X.; Song, Y.; Zhou, W.; Wang, Y. How Pore Hydrophilicity Influences Water Permeability? *Research* **2019**, *2019*, 2581241.

(30) Wang, S.; Xie, Y.; He, G.; Xin, Q.; Zhang, J.; Yang, L.; Li, Y.; Wu, H.; Zhang, Y.; Guiver, M. D.; Jiang, Z. Graphene Oxide Membranes with Heterogeneous Nanodomains for Efficient CO_2 Separations. *Angew. Chem., Int. Ed.* **2017**, *56*, 14246−14251.

(31) Sun, K.; Wang, C.; Dong, Y.; Guo, P.; Cheng, P.; Fu, Y.; Liu, D.; He, D.; Das, S.; Negishi, Y. Ion-Selective Covalent Organic

https://doi.org/10.1021/acsanm.2c03392
ACS Appl. Nano Mater. 2022, 5, 17632−17639

Framework Membranes as a Catalytic Polysulfide Trap to Arrest the Redox Shuttle Effect in Lithium−Sulfur Batteries. *ACS Appl. Mater. Interfaces* **2022**, *14*, 4079−4090.
(32) Yu, S.; Chen, Z.; Cheng, Q.; Lü, Z.; Liu, M.; Gao, C. Application of thin-film composite hollow fiber membrane to submerged nanofiltration of anionic dye aqueous solutions. *Sep. Purif. Technol.* **2012**, *88*, 121−129.
(33) Tang, H.; Ji, S.; Gong, L.; Guo, H.; Zhang, G. Tubular ceramic-based multilayer separation membranes using spray layer-by-layer assembly. *Polym. Chem.* **2013**, *4*, 5621−5628.
(34) Han, Y.; Xu, Z.; Gao, C. Ultrathin Graphene Nanofiltration Membrane for Water Purification. *Adv. Funct. Mater.* **2013**, *23*, 3693−3700.
(35) Wang, L.; Wang, N.; Li, J.; Li, J.; Bian, W.; Ji, S. Layer-by-layer self-assembly of polycation/GO nanofiltration membrane with enhanced stability and fouling resistance. *Sep. Purif. Technol.* **2016**, *160*, 123−131.
(36) Ding, J.; Wu, H.; Wu, P. Development of nanofiltration membranes using mussel-inspired sulfonated dopamine for interfacial polymerization. *J. Membr. Sci.* **2020**, *598*, No. 117658.
(37) Ding, W.; Zhuo, H.; Bao, M.; Li, Y.; Lu, J. Fabrication of organic-inorganic nanofiltration membrane using ordered stacking SiO_2 thin film as rejection layer assisted with layer-by-layer method. *Chem. Eng. J.* **2017**, *330*, 337−344.
(38) Zhao, G.; Wang, X.; Li, C.; Meng, H. Superhydrophilic alkynyl carbon composite nanofiltration membrane for water purification. *Appl. Surf. Sci.* **2020**, *508*, No. 144788.
(39) Mi, Y. F.; Wang, N.; Qi, Q.; Yu, B.; Peng, X. D.; Cao, Z. H. A loose polyamide nanofiltration membrane prepared by polyether amine interfacial polymerization for dye desalination. *Sep. Purif. Technol.* **2020**, *248*, No. 117079.
(40) Ding, J.; Wu, H.; Wu, P. Preparation of highly permeable loose nanofiltration membranes using sulfonated polyethylenimine for effective dye/salt fractionation. *Chem. Eng. J.* **2020**, *396*, No. 125199.
(41) Pan, F.; Guo, W.; Su, Y.; Khan, N. A.; Yang, H.; Jiang, Z. Direct growth of covalent organic framework nanofiltration membranes on modified porous substrates for dyes separation. *Sep. Purif. Technol.* **2019**, *215*, 582−589.
(42) Weng, R.; Huang, X.; Liao, D.; Xu, S.; Peng, L.; Liu, X. A novel cellulose/chitosan composite nanofiltration membrane prepared with piperazine and trimesoyl chloride by interfacial polymerization. *RSC Adv.* **2020**, *10*, 1309−1318.
(43) Zhao, S.; Zhu, H.; Wang, Z.; Song, P.; Ban, M.; Song, X. A loose hybrid nanofiltration membrane fabricated via chelating-assisted in-situ growth of Co/Ni LDHs for dye wastewater treatment. *Chem. Eng. J.* **2018**, *353*, 460−471.
(44) Hutter, J.; Iannuzzi, M.; Schiffmann, F.; VandeVondele, J. CP2K: atomistic simulations of condensed matter systems. *WIREs Comput. Mol. Sci.* **2014**, *4*, 15−25.
(45) VandeVondele, J.; Hutter, J. An efficient orbital transformation method for electronic structure calculations. *J. Chem. Phys.* **2003**, *118*, 4365−4369.
(46) VandeVondele, J.; Krack, M.; Mohamed, F.; Parrinello, M.; Chassaing, T.; Hutter, J. QUICKSTEP: Fast and accurate density functional calculations using a mixed Gaussian and plane waves approach. *Comput. Phys. Commun.* **2005**, *167*, 103−128.
(47) VandeVondele, J.; Hutter, J. Gaussian basis sets for accurate calculations on molecular systems in gas and condensed phases. *J. Chem. Phys.* **2007**, *127*, 114105.
(48) Grimme, S.; Antony, J.; Ehrlich, S.; Krieg, S. A consistent and accurate *ab initio* parametrization of density functional dispersion correction (DFT-D) for the 94 elements H-Pu. *J. Chem. Phys.* **2010**, *132*, 154104.
(49) Grimme, S.; Ehrlich, S.; Goerigk, L. Effect of the damping function in dispersion corrected density functional theory. *J. Comput. Chem.* **2011**, *32*, 1456−1465.
(50) Goedecker, S.; Teter, M.; Hutter, J. Separable dual-space Gaussian pseudopotentials. *Phys. Rev. B* **1996**, *54*, 1703−1710.
(51) Hartwigsen, C.; Goedecker, S.; Hutter, J. Relativistic separable dual-space Gaussian pseudopotentials from H to Rn. *Phys. Rev. B* **1998**, *58*, 3641−3662.
(52) Neese, F. The ORCA program system. *WIREs Comput. Mol. Sci.* **2012**, *2*, 73−78.
(53) Weigend, F.; Ahlrichs, R. Balanced basis sets of split valence, triple zeta valence and quadruple zeta valence quality for H to Rn: Design and assessment of accuracy. *Phys. Chem. Chem. Phys.* **2005**, *7*, 3297−3305.
(54) Weigend, F. Accurate Coulomb-fitting basis sets for H to Rn. *Phys. Chem. Chem. Phys.* **2006**, *8*, 1057−1065.
(55) Marenich, A. V.; Cramer, C. J.; Truhlar, D. G. Universal Solvation Model Based on Solute Electron Density and on a Continuum Model of the Solvent Defined by the Bulk Dielectric Constant and Atomic Surface Tensions. *J. Phys. Chem. B* **2009**, *113*, 6378−6396.

https://doi.org/10.1021/acsanm.2c03392
ACS Appl. Nano Mater. 2022, 5, 17632−17639